Non-Orthogonal Multiple Access for Hybrid VLC-RF Networks With Imperfect Channel State Information

Ahmed Al Hammadi , *Member, IEEE*, Paschalis C. Sofotasios , *Senior Member, IEEE*,
Sami Muhaidat , *Senior Member, IEEE*, Mahmoud Al-Qutayri , *Senior Member, IEEE*,
and Hany Elgala , *Senior Member, IEEE*

Abstract—This paper proposes a general framework for the energy efficiency analysis of a hybrid visible light communication (VLC) and Radio Frequency (RF) wireless system, in which both VLC and RF subsystems utilize non-orthogonal multiple access (NOMA) technology. The proposed framework is based on realistic communication scenarios as it takes into account the mobility of users and assumes imperfect channel-state information (CSI). In this context, tractable closed-form expressions are derived for the corresponding average sum-rate of NOMA-VLC and orthogonal frequency division multiple access (OFDMA)-VLC. It is shown extensively that incurred CSI errors have a considerable impact on the average energy efficiency of both NOMA-VLC and OFDMA-VLC systems. Hence, they should be taken into detailed account in the design of practical systems. We further demonstrate that the average energy efficiency of the hybrid NOMA-VLC-RF system outperforms the NOMA-VLC system under imperfect CSI. Respective computer simulations corroborate the derived analytic results, and interesting theoretical and practical insights are provided, which will be useful in the effective design and deployment of conventional VLC and hybrid VLC-RF systems.

Index Terms—Visible light communications, multiple access, imperfect CSI, sum-rate, hybrid wireless technologies.

NOMENCLATURE

List of Symbols

α	Power allocation factor
β_{RF}	RF Line of sight availability probability
β_{VLC}	VLC line of sight availability probability
ρ	Signal-to-noise ratio (SNR) at the transmitter
B_{RF}	RF Bandwidth
B_{VLC}	VLC bandwidth
e_k	Estimated error in the channel state estimation
i	Link index
k	User index
L	VLC Access Point Height
P_T	Total transmitted power of the VLC-RF network
P_{e}	Total electric power of LED
Q_{RF}	RF power consumption
Q_{VLC}	VLC power consumption
r_k	User's distance from the center of the cell
ψ_k	Angle of incidence
$\phi_{1/2}$	Semi-angle of the VLC AP
ϕ_k	Angle of irradiance
ψ_{FOV}	Receiver's field of view (FOV)
θ_i	User angle with respect to the VLC AP
$\hat{h}_k$	Estimated channel gain
h_k	Channel gain

I. INTRODUCTION

THE rapidly growing demand for data-intensive applications, such as video streaming, virtual reality (VR), and cloud computing, has led to an enormous growth in the global mobile data traffic, which results in annual traffic levels in the order of a zettabyte [2]. This poses challenging requirements for the fifth-generation (5G) of wireless networks and beyond, including massive connectivity, high throughput, low latency [3], and the references therein. In this context, several emerging technologies have been proposed for ultimately boosting the data rate. Examples of such technologies include massive multiple-input-multiple-output (MIMO) systems, ultra-dense networks, millimeter-wave communications, and visible light communications (VLC) [4].

VLC has recently attracted significant interest as a crucial technology for future wireless networks [4]. As a cost-effective and energy-efficient solution, VLC can potentially achieve considerably high data rates of the order of 100 Gbps [5]. Another

critical advantage of VLC is that it occupies a significantly larger portion of an unused spectrum spanning from 400THz to 800THz, which is immensely larger than the RF counterpart. It has been shown that such complementary approaches increase significantly the performance, efficiency, and robustness of wireless systems because they effectively combine the advantageous features of each single technology [5]. Moreover, a core advantage of VLC is that it is naturally secure due to the inherent characteristics of light, which cannot penetrate through walls and is confined within its area of illumination, offering a high degree of resource reuse. In addition, VLC is immune to electromagnetic interference (EMI) and, thus, to the existing RF systems, which is crucial, particularly in sensitive areas such as health-care centers, aircraft cabins, and other safety-critical environments [5].

It is also recalled that multiple access techniques have also been utilized extensively in modern wireless technologies to primarily enhance the spectrum efficiency and address the issue of spectrum crunch. To that end, they have ultimately emerged to be capable of improving several key challenging factors in wireless transmissions, such as energy and spectral efficiency, robustness, and reliability. In this context, non-orthogonal-multiple-access (NOMA) has attracted significant interests as a breakthrough technology for 5G systems and beyond. Since the main requirements of 5G networks revolve around high connectivity, low latency, and ultra-high-speed data rate, NOMA can be considered an effective enabling technology to address these requirements.

The most common variant of NOMA is power-domain NOMA, which assigns distinguished power levels to different users. The main feature of NOMA is that it enables multiple users to jointly share the entire frequency and time resources, which significantly improves the achievable spectral efficiency. The process of allocating different power levels to users is superposition coding (SC), while multi-user detection is achieved through successive interference cancellation (SIC) at the involved receivers. It is noted here that in power-domain based NOMA, the users with severe channel conditions are allocated more power, whereas less power is allocated for users with better channel conditions. The key motivation underlying this approach is to allocate particular power levels to different users according to the state of their channels and then apply SIC to eliminate the resulting interference and to ultimately achieve an acceptable throughput and fairness trade-off [6]–[9] and the references therein.

Based on the distinct advantages of these technologies, the application of NOMA in VLC systems has been investigated in several reported analyses. In more detail, the authors in [10] evaluated the performance of NOMA based multi-user VLC with a gain ratio power allocation strategy. There, they demonstrated that the sum-rate of VLC could be further enhanced by applying an adaptive tuning to the photo-detectors (PD), field-of-view (FOV), and the semi-angle of the light-emitting diodes (LEDs). The superiority of NOMA over OFDMA was shown in [11] through a performance comparison, taking into account the illumination constraints. Likewise, the performance of NOMA-based VLC with uniformly distributed users was evaluated in [12], assuming the idealistic case of perfect channel-state-information (CSI). In [13], the authors studied the data rate region of indoor VLC networks. In contrast, the authors in [14] investigated the error-rate performance of NOMA based VLC systems, with both perfect and imperfect CSI. The authors in [15] proposed a coordinated multi-attocell broadcast in VLC networks, where they designed it for the case of the imperfect CSI knowledge at the transmitter. Similarly, in [16] the authors proposed a precoder and equalizer design for an optical wireless MIMO system for VLC, in which they take into account the case of the imperfect channel state information. Another interesting study was reported in [39], where authors studied optimal power allocation for NOMA-VLC for both static users and mobile users under CSI uncertainties. In [40], the authors studied the bit error rate performance of NOMA-VLC under different modulation schemes. The study in [41] compared NOMA and OMA schemes in the VLC environment, where the users report positional information (vertical and horizontal) instead of reporting the full channel-state-information, which can significantly simplify the implementation.

More recently, the coexistence between indoor VLC and RF has attracted considerable attention due to its potential to provide enhanced performance in indoor communications [17]. In this context, the main motivations stem from the need to overcome the limitations of VLC in duplex transmission scenarios and to ensure ubiquitous service coverage. To this effect, Shao *et al.* [18] proposed a hybrid VLC-RF system, considering RF in the uplink. Likewise, Wang *et al.* [19] studied heterogeneous networks, which aims at providing high data rate VLC links alongside high-reliability RF links. The authors in [20] investigated load balancing in a hybrid VLC-RF system while considering user mobility and associated handover signaling. Also, it was shown [21] that the hybrid VLC-RF system can significantly enhance the overall coverage, which is a key requirement in VLC systems. Likewise, a recent study [22] for hybrid VLC-RF system has shown that this hybrid scheme achieves reduced outage probability and lower power consumption per area. In another study, the authors in [24] proposed a software-defined heterogeneous hybrid VLC-RF small-cell system. However, a key assumption in the study was the availability of perfect CSI, which is not a realistic assumption, particularly in highly demanding practical communication scenarios. In [27], the authors designed an online algorithm to minimize the power consumption of an indoor hybrid VLC-RF network while satisfying the constraint of the illumination level. In the same context, the authors in [28] studied optimal grouping for a hybrid NOMA VLC-RF network under perfect CSI. Likewise, [29] addressed the problem of optimal resource allocation in NOMA based hybrid VLC-RF with common backhaul to maximize the achievable data rate. In the context of vehicular communications, the authors in [37] proposed a robust hybrid VLC/RF model to manage resources to guarantee the Ultra-Reliable and Low-Latency of vehicular communication. Moreover, [38] have proposed a heterogeneous RF/VLC model to optimize link selection between RF and VLC. Finally, the authors in [30] studied the performance of NOMA based hybrid VLC-RF system in the context of simultaneous wireless and power transfer.

Nevertheless, despite its crucial importance, there have been sporadic results on the achievable energy efficiency levels of hybrid VLC-RF networks. Recently, the authors in [31] addressed energy consumption in a multihop VLC-RF network. Similarly, the contribution [32] studied the energy efficiency of an OFDMA based hybrid VLC-RF system through maximizing the system's power efficiency, which is defined as the total system rate per unit power. Motivated by the need for a theoretical framework for performance analysis of a hybrid NOMA-VLC-RF system, we investigate the average energy efficiency of the concerned system under practical considerations. We assume that the users are uniformly distributed and the CSI is imperfect. Based on this, the contributions of the present work are:

- We derive a novel average sum rate analytic expression for NOMA-VLC with uniformly distributed users under imperfect CSI. The derived expression is simple and does not require the computation of complex and often constrained functions.
- The corresponding average energy efficiency for hybrid NOMA-VLC/RF is derived assuming uniformly distributed users and under imperfect CSI. To the best of the author's knowledge, the derived expression for the average energy efficiency is novel.
- Capitalizing on the offered analytic results, we compare the performance of VLC-NOMA, VLC-OFDMA, hybrid VLC-RF NOMA, and provide valuable insights into the overall system performance, which could provide useful guidelines for practical designs.
- We quantify the impact of the CSI error on both NOMA-VLC and NOMA-VLC-RF systems, including its detrimental effect on the achievable average sum-rate and average energy efficiency. This provides particularly useful theoretical and practical insights on conventional and hybrid NOMA based VLC systems.

To the best of the authors' knowledge, the offered results have not been previously reported in the open technical literature.

The remainder of the paper is structured as follows: Section II describes the considered system and channel models comprehensively. Sections III and IV comprise the derivation of the average sum-rate for the considered NOMA based VLC and hybrid VLC-RF configurations, respectively, under imperfect CSI. The corresponding energy efficiency of the considered hybrid NOMA VLC-RF system is quantified in Section V, followed by the respective numerical results and useful discussions in Section . Finally, the paper is concluded with useful remarks in Section VI.

II. SYSTEM AND CHANNEL MODELS

As shown in Fig. 1, we consider a hybrid VLC-RF network operating in an indoor communication scenario which consists of one VLC AP (Access Point) and one RF AP. β_{RF} and β_{VLC} are LOS (line-of-sight) availability probabilities; those values can be chosen according to the expected ratio of LOS blockage for each AP. Without loss of generality, the focus of the present analysis is on the downlink communication scenario. In this context, the directional VLC AP covers a confined area, while
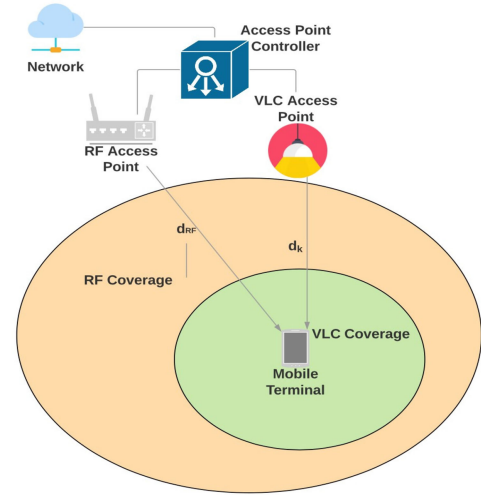

Fig. 1. The hybrid VLC-RF system model.

the RF AP covers a much wider area, using omni-directional antennas. A total number of K users are uniformly distributed, whereas powers denoted as Q_{RF} and Q_{VLC} are assumed for the RF and VLC APs, respectively. The sum represents the total power consumed by the hybrid network. Also, the VLC AP is installed in a ceiling of height L from the k_{th} end user located at the angle θ_i and radius r_i on the polar coordinate plane, whereas the maximum radius for the VLC AP coverage is denoted by r_e. The collaboration between RF and VLC is realized by the multi-homing capability, which enables mobile users to connect to more than one network and aggregate the resources from both the VLC network and the RF network [22]. It is noteworthy that multi-homing technique has been standardized in Release 12 by the name of "Dual Connectivity" [23]. It is also noted that this analysis adopts NOMA in both networks, where users share the entire RF bandwidth B_{RF} and VLC bandwidth B_{VLC}. To this effect, the P_T term denotes the total transmitted power of the VLC-RF network, namely

$$P_{R,i} + P_{V,i} \leq P_T, \tag{1}$$

where $P_{R,i}$ is the allocated power to the k_{th} user over the RF link and $P_{V,i}$ is the allocated power for the k_{th} user over the ith VLC link. It is noted here that although VLC channels direct and indirect signals, the energy of the reflected signal in the considered set up is considerably lower than that of the LOS [33]. Accordingly, this analysis considers only the LOS component of the optical channel gain.

A. VLC Channel Model

The signal transmitted by the VLC AP can be expressed as

$$x_i^{\mathrm{VLC}} = \sum_{i=1}^{K} \alpha_i \sqrt{P_e} s_i + I_{\mathrm{DC}}, \tag{2}$$

where P_e denotes the total electrical power of all the transmitted signals, I_{DC} is the LED DC bias which is essential for intensity modulation based optical baseband transmission, α_i is the power allocation coefficient for the corresponding k_{th} user. It
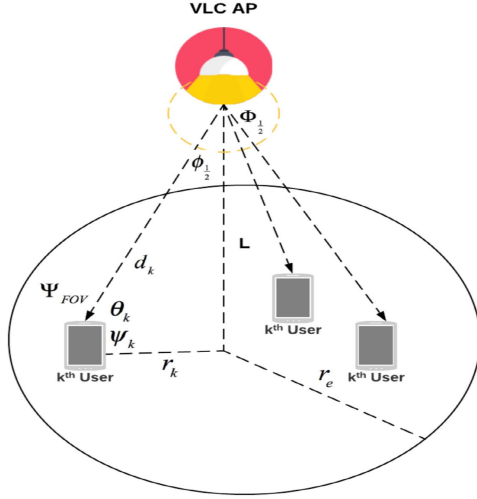
Fig. 2. VLC channel model.

is assumed that the transmitted signal for each user follows a uniform distribution with mean=0 and variance=1. We also assume that the signal transmitted by the ith VLC AP is subject to the following amplitude constraint

$$\left| x_i^{\text{VLC}} \right| \leq A_i. \tag{3}$$

According to the total power constraint of NOMA systems, the sum of power allocation coefficients must be unity, namely

$$\sum_{i=1}^{K} \alpha_i^2 = 1. \tag{4}$$

Subsequently, the power of the optical transmission for the LED can be expressed as

$$P_{\text{opt}} = \eta \text{E}[x] = \eta I_{\text{DC}}, \tag{5}$$

where η denotes the efficiency of the LED, which without loss of generality it is assumed to be unity. To this effect, the received signal at the k_{th} user can be expressed as

$$y_k^{\text{VLC}} = \sqrt{P_e} h_k \left(\sum_{i=1}^{k-1} a_i s_i + a_k s_k + \sum_{i=k+1}^{K} a_i s_i \right) + z_k, \tag{6}$$

where the channel gain h_k^{VLC} is given by

$$h_k^{\text{VLC}} = \frac{(m+1)AR_{\text{p}}}{2\pi d_k^2} \cos^m(\phi_k) T(\psi_k) g(\psi_k) \cos(\psi_k) \tag{7}$$

and z_k is the involved additive white Gaussian noise with mean = 0, and variance= $\sigma_k^2 = N_0 B$, with N_0 denoting the noise power spectral density (PSD), A is the area of the photo-detector, R_p denotes the responsivity of the photo-detector, and d_k is the Euclidean distance between the VLC AP and the k_{th} user. Also, $U(\psi_k)$ and $g(\psi_k)$ denote the optical filter gain and the optical concentrator, respectively. Notably, the above equation indicates that the channel gain h_k is inversely proportional to the distance of the k_{th} user. As shown in Fig. 2, the light emitted from the LED follows a Lambertian radiation pattern with order

$$m = -\frac{1}{\log_2(\cos(\phi_{1/2}))}, \tag{8}$$

where $\phi_{1/2}$ is the semi-angle of the VLC AP, ψ_{FOV} denotes the receiver's field of view (FOV), whereas ψ_k and ϕ_k denote the angle of incidence and the angle of irradiance, respectively.

It is recalled that, in NOMA-based systems, users with more favorable channel conditions are allocated less power, whilst users with less favorable channel conditions are allocated more power. Accordingly, the SIC decoding order is carried out according to the channel conditions of each user, in which users with worst channel conditions will decode their signal first, followed by users with better channel conditions, which implies that $\alpha_1 \geq \cdots \geq \alpha_k \cdots \geq \alpha_{K-1} \cdots \geq \alpha_K$.

Without loss of generality, we assume that the users in the considered set up are sorted in ascending order according to their channels, namely

$$\left| h_K^{\text{VLC}} \right| \geq \left| h_{K-1}^{\text{VLC}} \right| \geq \cdots \geq \left| h_k^{\text{VLC}} \right| \geq \cdots \geq \left| h_1^{\text{VLC}} \right|, \tag{9}$$

Therefore, in order to decode the signal successively, the k_{th} user performs SIC in order to remove the signal, s, of the other user(s) with stronger channel condition(s), whereby those signals are treated as noise. To this effect, the achievable data rate per bandwidth is expressed as follows [11]:

$$R_k = \begin{cases} \log_2 \left(1 + \frac{(h_k^{\text{VLC}} \alpha_k)^2}{\sum_{i=k+1}^{K}(h_k^{\text{VLC}} \alpha_i)^2 + \frac{1}{\rho}} \right), & k = 1, \ldots, K-1 \\ \\ \log_2 \left(1 + \rho(h_k^{\text{VLC}} \alpha_k)^2 \right), & k = K \end{cases} \tag{10}$$

where $\rho = P_e/N_0 B$ denotes the signal-to-noise ratio (SNR) at the transmitter. It is worth noting that (10) is conditioned on the requirement that each user performs the SIC operation successfully.

B. The VLC Channel Model for Uniformly Distributed Users

The angle of incidence, the angle of irradiance, and the Euclidian distance of the k_{th} user in terms of height L and radical distance r_k are given by

$$\cos(\phi_k) = \cos(\psi_k) = \frac{L}{d_k} \tag{11}$$

and

$$d_k = \sqrt{r_k^2 + L^2}. \tag{12}$$

Substituting these in (7), the DC gain for the LOS component can be determined, namely

$$h_k^{\text{VLC}} = \frac{\Xi(m+1)L^{m+1}}{(r_e^2 + L^2)^{\frac{m+3}{2}}}, \tag{13}$$

where

$$\Xi = \frac{AR_p U(\psi_k) g(\psi_k)}{2\pi} \tag{14}$$

is a constant. Furthermore, because of the uniform distribution of the users, the following probability density function (PDF) is used $f_{r_k}(r) = 2r/r_e$. Therefore, the PDF of the corresponding

channel gain is given by

$$f_{h_k}(t) = \frac{2\left(\Xi(m+1)L^{m+1}\right)^{\frac{2}{m+3}}}{r_e{}^2(p+3)t^{\frac{2}{m+3}+1}}, \quad t \in [\lambda_{\min}, \lambda_{\max}] \quad (15)$$

where

$$\lambda_{\min} = \frac{\Xi^2(m+1)^2 L^{2m+2}}{(r_e{}^2 + L^2)^{m+3}} \quad (16)$$

and

$$\lambda_{\max} = \frac{\Xi^2(m+1)^2 L^{2m+2}}{L^{2(m+3)}}. \quad (17)$$

Based on this and in order to obtain the corresponding cumulative distribution function (CDF), we integrate (15) over $[\lambda_{\min}, \lambda_{\max}]$, which yields

$$F_{h_k^2}(t) = 1 + \frac{L^2}{r_e^2} - \frac{(\Xi(m+1)L^{m+1})^{\frac{2}{m+3}}}{r_e^2 t^{\frac{1}{m+3}}}. \quad (18)$$

With the aid of order statistics [34], the PDF of the ordered channel gain denoted by $f'_{h_k}(t)$ can be obtained as

$$f'_{h_k^2}(t) = \frac{K! f_{h_k^2}(t)}{(k-1)!(K-k)!} F_{h_k^2}(t)^{k-1} \left[1 - F_{h_k^2}(t)\right]^{K-k}, \quad (19)$$

which can be equivalently expressed as:

$$f'_{h_k^2}(t) = \frac{\Omega}{m+3} \frac{K! t^{-\frac{1}{m+3}-1}}{(k-1)!(K-k)!}$$
$$\times \left(\frac{\Omega}{t^{\frac{1}{m+3}}} - \frac{L^2}{r_e{}^2}\right)^{K-k} \left(1 - \frac{\Omega}{t^{\frac{1}{m+3}}} + \frac{L^2}{r_e^2}\right)^{k-1} \quad (20)$$

where the constant $\Omega = \frac{1}{r_e^2}(C(m+1)L^{m+1})^{\frac{2}{m+3}}$.

Evidently, equation (20) has a convenient mathematical form owed to the involvement of only elementary functions.

C. The RF Channel Model

Following the same principles, the signal transmitted by the RF AP can be expressed as

$$x_i^{\mathrm{RF}} = \sum_{i=1}^{K} \sqrt{P_i^{\mathrm{RF}}} S_i^{\mathrm{RF}}, \quad (21)$$

where S_i^{RF} denotes the transmitted symbol of the k_{th} user. We also let h_K^{RF} denote the channel gain from the RF AP to the k_{th} user. Accordingly, it is assumed that h_k^{RF} of the K users are perfectly known and are sorted as

$$\left|h_K^{\mathrm{RF}}\right| \geq \left|h_{K-1}^{\mathrm{RF}}\right| \geq \cdots \geq \left|h_k^{\mathrm{RF}}\right| \geq \cdots \geq \left|h_1^{\mathrm{RF}}\right|, \quad (22)$$

with the assumption that the SIC decoding order is carried out according to the the channel conditions of each user, as discussed earlier. Moreover, users with good channels conditions are allocated less power, and lower-order users are allocated more power. By applying the NOMA principle, the signal received by

the k_{th} user in the RF channel can be represented as

$$y_k^{\mathrm{RF}} = h_k^{\mathrm{RF}} \sum_{i=1}^{K} \sqrt{\alpha_{i,r} P} s_{i,r} + z_{i,r}, \quad (23)$$

where h_k^{RF} stands for the RF channel gain, namely

$$h_k^{\mathrm{RF}} = \frac{H_k}{d_k^{\chi/2}}, \quad (24)$$

where $H_k \sim \mathcal{CN}(0, 1)$ with d_k denoting the distance between the RF AP and the k_{th} user, and χ denoting the RF path loss exponent. It is noted here that although the system can achieve its optimal performance when the CSI channel is considered perfect, obtaining a perfect or near-perfect CSI is not feasible in a practical communication environment. Subsequently, it is crucial to obtain an insight into the system performance under realistic conditions in which the CSI channel can be typically imperfect.

D. Imperfect CSI Model

Unlike the majority of the previous related contributions, which assumed perfect CSI knowledge, this work assumes the practical case of imperfect CSI for the underlying RF-VLC system model. Typically, the CSI can be obtained at the receivers through pilot symbols. In this process, the channel coefficients are sent to the transmitter through an RF or an infrared (IR) uplink, where channel uncertainty increases as the noise increases in uplink and downlink channels. Furthermore, the channel uncertainty is further increased due to quantization errors that are incurred from the imperfect digital-to-analog, analog-to-digital process, which is ultimately detrimental to the overall system performance. It is noted here that the present analysis adopts the noisy CSI model as in [14], which considers the resultant CSI error regardless of the sources that caused the error i.e. location uncertainty, orientation uncertainty, and LED half-angle uncertainty.

1) VLC Imperfect CSI Model: The channel coefficient for the VLC link can be modeled by using the minimum mean squared error (MMSE) estimation method, yielding[14]

$$h_k^{\mathrm{VLC}} = \hat{h}_k^{\mathrm{VLC}} + e_k^{\mathrm{VLC}}, \quad (25)$$

where $\hat{h}_k \sim \mathcal{N}(0, 1 - \sigma_e^2)$ is the estimated channel gain and e_k denotes the estimated error in the channel which follows a Gaussian distribution with mean $= 0$ and variance$= \sigma_e^2$. It is worth noting that the random variables $\hat{h}_k$ and e_k are uncorrelated and the maximum achievable data rate for the VLC channel according to Shannon formula is given by

$$C_{\mathrm{VLC}} = B_{\mathrm{VLC}} \log_2(1 + \mathrm{SINR}), \quad (26)$$

where B_{VLC} is the bandwidth of the channel. Hence, the signal-to-interference-plus-noise ratio (SINR) of the k_{th} user over the VLC channel under imperfect CSI is given by

$$\mathrm{SINR}_k^{\mathrm{VLC}} = \begin{cases} \frac{\hat{h}_k^2 \alpha_k^2}{\sum_{i=k+1}^{K} \hat{h}_k^2 \alpha_i^2 + \frac{1}{\rho} + \sigma_e^2}, & k = 1, \ldots, K-1 \\ 1 + \rho \hat{h}_k^2 \alpha_k^2 + \sigma_e^2, & k = K \end{cases}$$

$$(27)$$

By substituting (27) into (26), the maximum achievable data rate for the k_{th} user under imperfect CSI is given by

$$R_k^{\text{VLC}} = \begin{cases} \log_2\left(1 + \frac{\hat{h}_k^2 \alpha_k^2}{\sum_{i=k+1}^K \hat{h}_k^2 \alpha_i^2 + \frac{1}{\rho} + \sigma_e^2}\right), & k = 1, \ldots, K-1 \\ \log_2\left(1 + \rho \hat{h}_k^2 \alpha_k^2 + \sigma_e^2\right), & k = K \end{cases}$$

(28)

which also has a simple algebraic representation.

2) VLC Imperfect CSI Model With Amplitude-Constraint: Following [42], the lower bound on the achievable data rate expression for VLC can be obtained as follows

$$R_k^{\text{VLC}} \geq \begin{cases} \log_2\left(1 + \frac{2\pi\sigma_k^2 + \hat{h}_k^2 e^{1+2(\zeta_k + \gamma_k \alpha_k)}}{2\pi\sigma_k^2 + 2\pi\sum_{i=k+1}^K \hat{h}_k^2 \alpha_i^2 + \frac{1}{\rho} + \sigma_e^2}\right), \\ \text{for } k = 1, \cdots, K-1 \\ \log_2\left(1 + \frac{2\pi\sigma_k^2 + \rho\hat{h}_k^2 e^{1+2(\zeta_k + \gamma_k \alpha_j)} + \sigma_e^2}{2\pi\sigma_k^2}\right), \\ \text{for } k = K \end{cases}$$

(29)

where the parameters ζ_k, γ_k, and η_k are solutions of the following equations [42]

$$T_k(A_k) - T_k(-A_k) = e^{1+\zeta_k},$$

$$\eta_k \left(e^{A_k(\eta_k - \gamma_k A_k)} - e^{1+\zeta_k} - e^{-A_k(\eta_k + \gamma_k A_k)}\right) = 0,$$

and

$$e^{A_k(\eta_k - \gamma_k A_k)} \left((\eta_k - 2\gamma_k A_k)e^{-2A_k \eta_k} - \eta_k - 2\gamma_k A_k\right)$$
$$+ (\eta_k^2 + 2\gamma_k)e^{1+\zeta_k} = 4\gamma_k^2 \alpha_k e^{1+\zeta_k}.$$

The A_k in the above representation denotes the amplitude constraint for the transmitted signal, and the function T_k is defined by

$$T_k(X) = \sqrt{\pi} \frac{e^{\frac{\eta_k^2}{4\gamma_k}} \text{erf}\left(\frac{\eta_k + 2\gamma_k X}{2\sqrt{\gamma_k}}\right)}{2\sqrt{\gamma_k}}$$

(30)

where erf(.) is the error function, which can expressed as

$$\text{erf}(x) \triangleq \frac{2}{\sqrt{\pi}} \int_0^x e^{-t^2} dt$$

(31)

and is related to the well-known one dimensional Gaussian $Q-$function as $\text{erf}(x) = 1 - 2Q(x\sqrt{2})$.

3) RF Imperfect CSI Model: The channel coefficient for the RF link can be estimated using the MMSE channel estimation model as follows:

$$h_k^{\text{RF}} = \hat{h}_k^{\text{RF}} + e_k^{\text{RF}},$$

(32)

where $h_k^{\text{RF}} \sim \mathcal{CN}(0, 1 - \sigma_e^2)$ represents the estimated channel gain and e_k^{RF} denotes the estimated error in the channel, which is following a complex Gaussian distribution with mean=0 and variance= σ_e^2. Also, it is assumed again that the random variables h_k^{RF} and e_k^{RF} are uncorrelated. To this effect, the maximum achievable data rate for the channel according to Shannon formula is readily expressed as

$$C_{\text{RF}} = B_{\text{RF}} \log_2(1 + \text{SINR}),$$

(33)

where B_{RF} is the bandwidth of the RF channel. Also, the SINR for the k_{th} user over an RF channel under imperfect CSI is expressed as

$$\text{SINR}_k^{\text{RF}} = \begin{cases} \frac{\alpha_k(\hat{h}_k^{\text{RF}})^2}{\sum_{i=k+1}^K \alpha_i(\hat{h}_k^{\text{RF}})^2 + \frac{1}{\rho} + \sigma_e^2}, & k = 1, \cdots, K-1 \\ 1 + \rho\alpha_k(\hat{h}_k^{\text{RF}})^2 + \sigma_e^2, & k = K \end{cases}$$

(34)

By substituting (34) into (33), the maximum achievable data rate for the k_{th} user under imperfect CSI is given by

$$R_k^{\text{RF}} = \begin{cases} \log_2\left(1 + \frac{\alpha_k(\hat{h}_k^{\text{RF}})^2}{\sum_{i=k+1}^K \alpha_i(\hat{h}_k^{\text{RF}})^2 + \frac{1}{\rho} + \sigma_e^2}\right), & k = 1, \cdots, K-1 \\ \log_2\left(1 + \rho\alpha_k(\hat{h}_k^{\text{RF}})^2 + \sigma_e^2\right), & k = K \end{cases}$$

(35)

which has similarly a simple algebraic representation as to the maximum achievable data rate in the VLC channel.

III. AVERAGE SUM-RATE OF VLC UNDER IMPERFECT CSI

In this section, we derive a closed-form solution for the average sum-rate of NOMA based VLC under imperfect CSI. Additionally, the sum-rate for the corresponding OFDMA-based VLC system is derived for both perfect and imperfect CSI for the sake of benchmarking as it is subsequently compared with the results of the considered set up.

A. Average Sum-Rate of Uniformly Distributed users

In this subsection, the average sum-rate is derived for both NOMA and OFDMA VLC systems under imperfect CSI, assuming uniformly distributed users.

1) NOMA Sum-Rate With Imperfect CSI: The NOMA based sum-rate with imperfect CSI is introduced in the following theorem.

Theorem 1: For a K number of uniformly distributed users and an arbitrary power allocation strategy, the average sum-rate of NOMA-VLC under imperfect CSI is expressed by the exact closed-form expression in (36), shown at the bottom of this page, where

$$\Omega(x, y, z) = \left(x(y+1) + \frac{1}{z^{y+1}}\right)\ln(1 + zx)$$
$$+ \sum_{i=1}^{y+1}\left(\frac{-x_{y-i+2}(1)^{i-1}}{(y-i+2)z^{i-1}}\right).$$

(37)

Proof: The average sum-rate of NOMA VLC under imperfect CSI and amplitude-constraint is given by

$$\tilde{R}_{\text{VLC}}^{\text{NOMA}} \geq \sum_{k=1}^M E[R_k]$$

(38)

$$\geq \sum_{k=1}^{K-1} \int_{\lambda_{\min}}^{\lambda_{\max}} \log_2\left(1 + \frac{2\pi\sigma_k^2 + \hat{h}_k^2 e^{1+2(\zeta_k + \gamma_k \alpha_k)}}{2\pi\sigma_k^2 + 2\pi\sum_{i=k+1}^K \hat{h}_k^2 \alpha_i^2 + \frac{1}{\rho} + \sigma_e^2}\right)$$
$$\times f'_{h_k^2}(t)dt$$

$$+ \int_{\lambda_{\min}}^{\lambda_{\max}} \log_2 \left(1 + \frac{2\pi\sigma_k^2 + \rho \hat{h}_k^2 e^{1+2(\zeta_k + \gamma_k \alpha_j)} + \sigma_e^2}{2\pi\sigma_k^2} \right)$$

$$\times f'_{h_K^2}(t)\mathrm{dt}. \tag{39}$$

Notably, it is pointed out that (39) does not yield a tractable solution that can give deep insights into the system performance. Consequently, in the subsequent analysis and in order to obtain meaningful insights, this assumption is relaxed.

To this effect, following [12], the average sum-rate of NOMA VLC under imperfect CSI can be expressed as

$$\hat{R}_{\mathrm{VLC}}^{\mathrm{NOMA}} = \sum_{k=1}^{M} E[R_k] \tag{40}$$

$$= \sum_{k=1}^{K-1} \underbrace{\int_{\lambda_{\min}}^{\lambda_{\max}} \log_2 \left(1 + \frac{(\alpha_k)^2 t}{\sum_{i=k+1}^{K} (\alpha_i)^2 t + \frac{1}{\rho} + \sigma_e^2} \right) f'_{h_k^2}(t)\mathrm{dt}}_{Q_s}$$

$$+ \underbrace{\int_{\lambda_{\min}}^{\lambda_{\max}} \log_2 \left(1 + \rho \alpha_K^2 t + \sigma_e^2 \right) f'_{h_K^2}(t)\mathrm{dt}}_{V_s} \tag{41}$$

where $E[*]$ is the expectation operator, Q_s denotes the ergodic data rate for the k_{th} user, $k \in \{1, \cdots, K-1\}$, and V_s denotes the ergodic data rate for the k_{th} user. Hence, it is apparent that deriving a closed-form expression to (40) is subject to analytically solving the involved two integrals. To that end, applying the binomial expansion in the above, V_s can be given by:

$$V_s = \frac{\Xi K}{2(m+3)} \sum_{l=0}^{K-1} \frac{(K-1)!(-\Xi)^l}{l!(K-1-l)!} \left(\frac{L^2}{r_e^2} + 1 \right)^{K-1-l}$$

$$\times \underbrace{\int_{\lambda_{\min}}^{\lambda_{\max}} \log_2 \left[1 + \left(\rho(\alpha_k)^2 t + \sigma_e^2 \right) \right] t^{-\frac{l+1}{m+3}-1} \mathrm{dt}}_{Vsi}. \tag{42}$$

Evidently, we have to solve the integral V_{si} in order to deduce the final solution. To this end, using [36, 2.729.l], and by defining

$$b_1 = \rho(\alpha_k)^2 + \sigma_e^2 \tag{43}$$

and

$$v_1 = -\frac{l+1}{m+3} - 1 \tag{44}$$

V_{si} can be readily obtained as follows:

$$V_{si} = \frac{1}{\ln(2)(v_1+1)} \left(t^{v_1+1} - \frac{(-a)^{v_1+1}}{\left(\rho(\alpha_k)^2 + \sigma_e^2 \right)^{v_1+1}} \right)$$

$$\times \ln \left(1 + \left(\rho(\alpha_k)^2 + \sigma_e^2 \right) t \right)$$

$$+ \frac{1}{\ln(2)(v_1+1)} \sum_{i=1}^{v_1+1} \left(\frac{(-1)^i t^{v_1-i+2} a^{i-1}}{(v_1-i+2)\left(\rho(\alpha_k)^2 + \sigma_e^2 \right)^{i-1}} \right). \tag{45}$$

Based on this and substituting (45) into (42), the following expression is obtained

$$V_s = \Xi K \sum_{l=0}^{K-1} \left\{ \frac{(-1)^l (K-1)! \Xi^l}{l!(K-1-l)!(v_1+1)} \left(\frac{L^2}{r_e^2} + 1 \right)^{K-1-l} \right.$$

$$\left. \times \frac{\Omega(\lambda_{\max}, b_1, v_1) - \Omega(\lambda_{\min}, b_1, v_1)}{\ln(2)(m+3)} \right\}, \tag{46}$$

where

$$\Omega(x, y, z) = \left(x_{y+1} - \frac{(-1)^{y+1}}{(z)^{y+1}} \right) \ln(1 + (z)x)$$

$$+ \sum_{i=1}^{v_1+1} \left(\frac{(-1)^i x_{v_1-i+2}(1)^{i-1}}{(y-i+2)(z)^{i-1}} \right). \tag{47}$$

Similarly, by applying binomial expansion for the integral Q_s in (41), we obtain

$$Q_s = \frac{\Xi}{(m+3)} \sum_{k=1}^{K-1} \sum_{p=0}^{k-1} \sum_{q=0}^{K-k} \frac{K! \Xi^{p+q}(-1)^{p+K-k-q}}{p!(k-1-p)q!(K-k-q)!}$$

$$\times \left(\frac{L^2}{r_e^2} + 1 \right)^{k-1-p} \left(\frac{L^2}{r_e^2} \right)^{K-k-q} Q_{si}, \tag{48}$$

where

$$Q_{si} = \int_{\lambda_{\min}}^{\lambda_{\max}} \log_2 \left(1 + \frac{(\alpha_k)^2 t}{\sum_{i=k+1}^{K} (\alpha_i)^2 t + \frac{1}{\rho} + \sigma_e^2} \right) \mathrm{dt}. \tag{49}$$

Next, Q_{si} can be deduced using the same previous steps. Hence, by first defining the following parameters:

$$b_2 = \frac{\rho((\alpha_k)^2 - \sigma_e^2)}{\sum_{i=k+1}^{K} \alpha_i^2} \tag{50}$$

$$\hat{R}_{\mathrm{VLC}}^{\mathrm{NOMA}} = \frac{\Xi K}{\ln(2)(m+3)} \left\{ \sum_{l=0}^{K-1} \frac{(K-1)!(-\Xi)^l}{l!(K-1-l)!(v_1+1)} \left(\frac{L^2}{r_e^2} + 1 \right)^{K-1-l} [\Omega(\lambda_{\max}, v_1, b_1) - \Omega(\lambda_{\min}, v_1, b_1)] \right.$$

$$\left. + \sum_{k=1}^{K-1} \sum_{p=0}^{k-1} \sum_{q=0}^{K-k} \frac{(K)!(\Xi)^{p+q}(-1)^{p+K-k-q}}{p!(k-1-p)q!(K-k-q)!} \left(\frac{L^2}{r_e^2} + 1 \right)^{k-1-p} \left(\frac{L^2}{r_e^2} \right)^{K-k-q} [\Omega(\lambda_{\max}, v_2, b_2) - \Omega(\lambda_{\min}, v_2, b_2)] \right\} \tag{36}$$

and

$$v_2 = -\frac{p+q+1}{m+3} - 1 \tag{51}$$

and carrying out some manipulations yields (52), shown at the bottom of this page. Hence, by substituting (52) and (46) into (41) yields (36), which completes the proof. ∎

It is noteworthy that the results reported in [11] include complex and constrained special functions like the hypergeometric function 2F1. In addition, they are limited to the simplistic assumption of perfect CSI knowledge as they do not take into account any incurred CSI errors. Hence, the consideration of CSI errors in Theorem 1 is more practical and, therefore, more useful when considering realistic communication scenarios in emerging technologies that are typically characterized by demanding requirements and stringent quality of service targets. Another advantage of the offered result in Theorem 1 is its simple algebraic form since it does not include special functions. This renders it convenient to perform analyses both numerically and analytically.

2) OFDMA Sum-Rate With Imperfect CSI: In what follows, we quantify the sum-rate for the corresponding OFDMA counterpart.

Theorem 2: For K number of uniformly distributed users, and an arbitrary power allocation strategy, the average sum-rate of OFDMA VLC under imperfect CSI can be expressed by the closed-form representation in (53), shown at the bottom of this page.

Proof: The average sum-rate of OFDMA VLC under imperfect CSI is obtained by the following representation:

$$\hat{R}_{\text{VLC}}^{\text{OFDMA}} = \sum_{k=1}^{K} \int_{\lambda_{\min}}^{\lambda_{\max}} \log_2\left(1 + \frac{\rho w_k t}{b_{nk}(1 + \rho\sigma_e^2)}\right) \frac{w_k f'_{h_k^2}(t)}{2} dt \tag{54}$$

where w_k is the portion of bandwidth allocated by the k_{th} user, and b_{n_k} is the portion of power allocated by the k_{th} user. By applying the binomial expansion, the average sum-rate of OFDMA VLC under imperfect CSI is given by (55), shown at

the bottom of the next page, where T_s can be expressed as

$$T_s = \frac{\Omega(\lambda_{\max}, v_3, b_3) - \Omega(\lambda_{\min}, v_3, b_3)}{2\ln(2)}. \tag{56}$$

Subsequently, using [36, 2.729.1], and by defining:

$$b_3 = \frac{\rho w_k}{b_{nk}(1 + \rho\sigma_e^2)} \tag{57}$$

and

$$v_3 = -\frac{p+q+1}{(m+3)} - 1, \tag{58}$$

it follows that the exact closed-form expression in (53) is obtained by substituting (56) into (55), which completes the proof of the theorem.

IV. AVERAGE SUM-RATE OF NOMA-RF UNDER IMPERFECT CSI

The average sum-rate of a NOMA based RF system with imperfect CSI can be obtained using (59), shown at the bottom of the next page, where [35]

$$\phi(x) = \sum_{t_1+\cdots+t_n=j} \frac{j!}{t_1! t_2! \cdots t_n!} \prod_{i=1}^{n} \left(\left|\sin\frac{2i-1}{2n}\pi\right| x_i\right)^{t_i} h(x) \tag{60}$$

with j denoting the summation of all sequences of non-negative integer indices from t_1 until t_n, and

$$h(x) = \exp\left(\frac{(\sigma_z^2 + P_{R,k}\sigma_\varepsilon^2)}{P_{R,k}z} \sum_{i=1}^{n} \frac{t_i}{x_i^{-\beta_R} - \sigma_\varepsilon^2}\right)$$
$$\times E_1\left(\frac{(\sigma_z^2 + P_{R,k}\sigma_\varepsilon^2)}{P_{R,k}z} \sum_{i=1}^{n} \frac{t_i}{x_i^{-\beta_R} - \sigma_\varepsilon^2}\right) \tag{61}$$

where $E_1(\cdot)$ denotes the exponential integral [36]. This function can be readily computed because it is a standard built in function in scientific software packages such as MAPLE, MATLAB and MATHEMATICA.

$$Q_s = \sum_{k=1}^{K-1} \sum_{p=0}^{k-1} \sum_{q=0}^{K-k} \frac{K! \Xi^{p+q+1}(-1)^{p+K-k-q}(L^2 + r_e^2)^{k-p-1}L^{2(K-k-q)}}{\ln(2)(m+3)p!(k-1-p)q!(K-k-q)!r_e^{2(K-q-p-1)}} \times \{\Omega(\lambda_{\max}, b2, v2) - \Omega(\lambda_{\min}, b2, v2)\} \tag{52}$$

$$\hat{R}_{\text{VLC}}^{\text{OFDMA}} = \sum_{k=1}^{K} \sum_{p=0}^{k-1} \sum_{q=0}^{K-k} \frac{K! \Xi^{p+q+1}(-1)^{p+K-k-q} [\Omega(\lambda_{\max}, v_3, b_3) - \Omega(\lambda_{\min}, v_3, b_3)]}{2\ln(2)p!(k-1-p)q!(K-k-q)!(v_3+1)(m+3)} \left(\frac{L^2}{r_e^2}\right)^{K-k-q} \left(\frac{L^2}{r_e^2} + 1\right)^{k-1-p} \tag{53}$$

$$\hat{R}_{\text{VLC}}^{\text{OFDMA}} = \frac{\Xi}{2(m+3)} \sum_{k=1}^{K} \sum_{p=0}^{k-1} \sum_{q=0}^{K-k} \frac{K! \Xi^{p+q}(-1)^{p+K-k-q}}{p!(k-1-p)q!(K-k-q)!} \left(\frac{L^2}{r_e^2} + 1\right)^{k-1-p} \left(\frac{L^2}{r_e^2}\right)^{K-k-q}$$
$$\times \sum_{k=1}^{K} \underbrace{\int_{\lambda_{\min}}^{\lambda_{\max}} \frac{1}{2} w_k \log_2\left(1 + \frac{w_k \rho t}{b_{nk}\sigma_e^2}\right) f'_{h_k^2}(t)dt}_{T_s} \tag{55}$$

To the best of the author's knowledge, the derived results are novel. Capitalizing on the results, the performance of the considered setup in terms of the average sum-rate of NOMA-RF under imperfect CSI is quantified in detail in the numerical results section, where useful theoretical and practical insights are developed.

V. AVERAGE ENERGY EFFICIENCY OF HYBRID NOMA VLC-RF SYSTEM

Next, we derive the average sum-rate and the energy efficiency of the NOMA-VLC-RF network, assuming imperfect knowledge of the CSI. Following [32], we define the total average sum-rate in a hybrid VLC-RF network as follows:

$$R_{\text{SUM}} = B_{\text{RF}} \left(\beta_{\text{RF}} \hat{R}_{\text{RF}}^{\text{NOMA}} \right) + B_{\text{VLC}} \left(\beta_{\text{VLC}} \hat{R}_{\text{VLC}}^{\text{NOMA}} \right), \tag{62}$$

where β_{RF} is the probability of available LOS (dominant) component for the RF link, and β_{VLC} is the corresponding LOS availability probability for the VLC link. It is noted that the above representation is useful in determining the average energy efficiency of the considered hybrid set up.

Corollary 2.1: The average energy efficiency of the considered hybrid VLC-RF network can be determined as follows:

$$\hat{\xi} = \frac{B_{\text{RF}} \left(\beta_{\text{RF}} \hat{R}_{\text{RF}}^{\text{NOMA}} \right) + B_{\text{VLC}} \left(\beta_{\text{VLC}} \hat{R}_{\text{VLC}}^{\text{NOMA}} \right)}{Q_{\text{VLC}} + Q_{\text{RF}} + \sum_{i=1}^{N} P_{\text{RF},i}}. \tag{63}$$

Proof: The average sum-rate of the investigated set up is expressed in bits per second (bits/s), whereas the energy efficiency metric is expressed in terms of bit per joule. Accordingly, the energy efficiency is given by

$$\xi = \frac{R_{\text{SUM}}}{Q_{\text{VLC}} + Q_{\text{RF}} + \sum_{i=1}^{N} P_{\text{RF},i}}, \tag{64}$$

where R_{Sum} stands for the maximum achievable sum-rate of NOMA-VLC-RF and $\sum_{i=1}^{N} P_{\text{RF},i}$ is the total transmission power of the RF network for N users. Based on this and by substituting (62) into (64), equation (63) is deduced, which completes the proof. ∎

VI. RESULTS AND DISCUSSION

In this section, we utilize the derived analytic results in the proposed theoretical framework alongside the corresponding Monte Carlo simulation for validation purposes. To that end and unless otherwise stated, the analytical results in the presented figures are represented by solid lines whereas the corresponding Monte Carlo simulation results by are represented by markers.

TABLE I
SIMULATION PARAMETERS

| Parameter	Value
Vertical separation between the LED and PDs, L	2.15 m
Cell radius, r_e	3.6 m
LED semi-angle	45°
Total signal power, P_e	0.25 W
PD FOV, Ψ_{fov}	60°
PD responsivity R_p	0.4 A/W
PD detection area, A	1 cm^2
Reflective index, n	1.5
Optical filter gain, T	1
Signal bandwidth, B	20 MHz
VLC AP fixed power consumption, Q_{VLC}	4 Watt
RF AP fixed power consumption, Q_{RF}	6.7 Watt
Noise PSD, N_0	20^{-21} A^2 /Hz
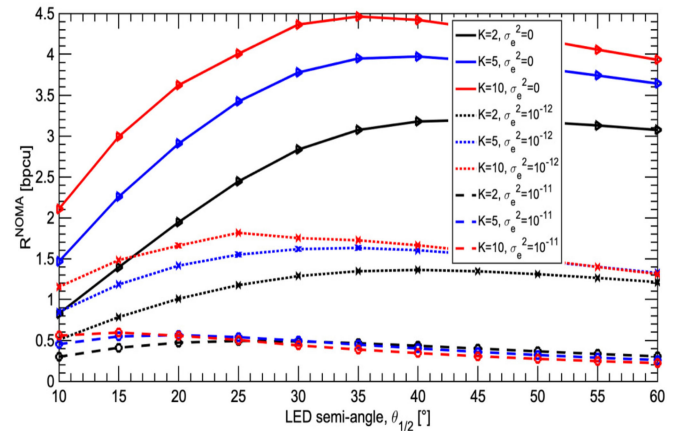
Fig. 3.   Sum-rate vs. semi-angle for LED in NOMA-VLC system.

Our results exhibit a perfect match between analysis and simulations in all consider cases, which justifies the validity of the derivations. Based on [27], the default simulation parameters are depicted in Table I, unless otherwise specified.

A. Sum-Rate of VLC Using NOMA/OFDMA

Fig. 3 demonstrates the achieved sum-rate as a function of the LED semi-angle in the VLC system with a different number of users, and different σ_e values. It is clear from Fig. 3 that the CSI estimation error impacts the overall system performance considerably. Specifically, it is shown that the maximum sum-rate is decreased from 3.19 bits per channel unit (bpcu) to 1.36 bpcu, a 57% decrease ratio for the $K = 2$ case. As for the considered cases of 5 and 10 users, almost the same reduction ratio applies as the CSI estimation error is increased. This is due to the nature of the VLC attocell and uniformly distributed users. Specifically, when the LED semi-angle is small, the light

$$\hat{R}_{\text{RF}}^{\text{NOMA}} \approx \sum_{k=2}^{K} \sum_{r=0}^{k-1} \binom{K}{k} \binom{k-1}{r} \frac{k(-1)^r}{\ln(2)(r+k)} \sum_{j=1}^{r+K-k+1} \binom{r+K-k+1}{j} \frac{(-1)^j \pi^j}{n^j D^j} \phi(\beta_{R,k-1})$$

$$- \sum_{k=1}^{K} \sum_{r=0}^{k-1} \binom{K}{k} \binom{k-1}{r} \frac{k(-1)^r}{\ln(2)(r+k)} \sum_{j=1}^{r+K-k+1} \binom{r+K-k+1}{j} \frac{(-1)^j \pi^j}{n^j D^j} \phi(\beta_{R,k}) \tag{59}$$
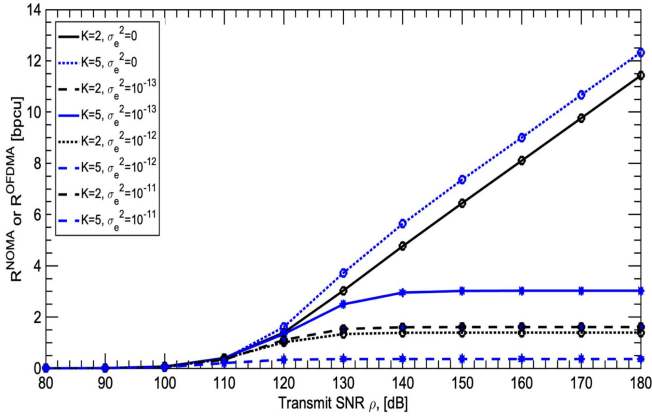
Fig. 4.   Sum-rate vs. transmit SNR in NOMA-VLC system.

Fig. 5.   Sum-rate vs. transmit SNR for NOMA-VLC and OFDMA-VLC.

Fig. 6.   Sum-rate vs. the number of users for NOMA-VLC.

intensity concentrated on the central users only, limiting the performance of the network. However, as the LED semi-angle increases, the light intensity is no longer a narrow beam but rather distributed uniformly across the entire cell. Accordingly, there is an optimal LED semi-angle in which the performance of the network is maximum. Moreover, it is noticed that high estimation errors lead to a diminishing difference between the sum-rate of 2, 5, and 10 users. In other words, as the CSI estimation error increases, the channels between the users become less distinctive, which leads to minimal performance gain as the number of users increases. This is a critical finding since NOMA, and VLC scenarios rely crucially on the state of the involved wireless channels. In the same context, Fig. 4 illustrates the corresponding sum-rate as a function of the transmit SNR ρ for $K = 2$ and $K = 5$ and different σ_e values. The first key observation is that the impact of the CSI error is rather minimal in the region of low SNR, and it becomes more pronounced as the transmit SNR ρ increases. Secondly, there is an upper ceiling bound for the sum-rate, leading to a flat sum-rate value. Next, the cost of CSI errors is increased as the transmit SNR increases. For instance, at 180 dB for $K = 5$, the CSI error of -120 dB decreases the sum-rate from 12 bpcu to 3.9 bpcu, whereas in the 150 dB case, the sum-rate is reduced from 7.5 bpcu to 3.9 bpcu. Finally, in the case of CSI -110 dB, the performance is almost flat with a very low sum-rate (around 0.2 bpcu). The CSI errors become the performance bottleneck in the VLC system since imperfect channel estimation leads to incorrect channel ordering, which is crucial for SIC and data detection. This demonstrates the importance of taking the incurred CSI imperfections into account during the design process to achieve reliable and robust operation of NOMA based VLC systems.

Fig. 5 illustrates the sum-rate versus ρ for both NOMA-VLC and OFDMA-VLC setups with $K = 5$ users under different CSI error values. As expected, NOMA outperforms OFDMA throughout the entire SNR range considered. Moreover, the performance gain of NOMA over OFDMA is superior under the perfect CSI scenario. For example, in the case of $\rho = 180$ dB, the sum-rate of NOMA is almost double the sum-rate of OFDMA (12.1 for the former vs. 6.4 for the latter). Interestingly, for the SNR region between 110 dB and 130 dB, NOMA with
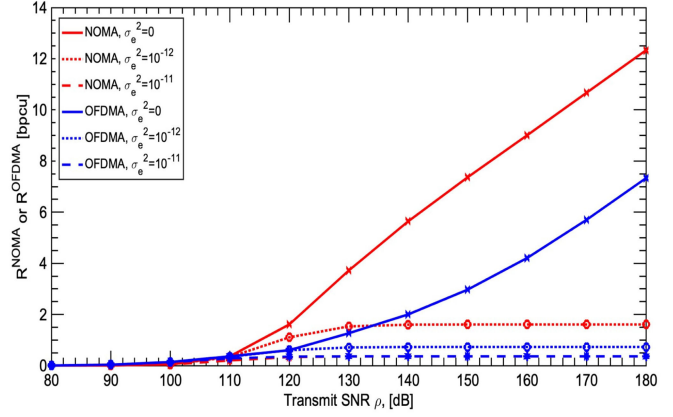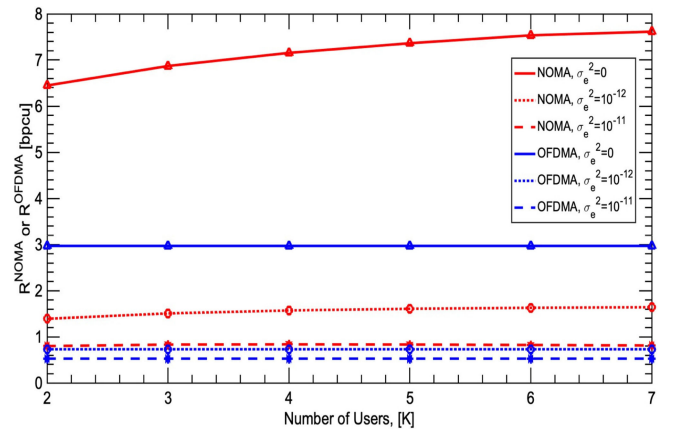
imperfect CSI and -120 dB outperforms OFDMA with perfect CSI. This can be explained by the fact that the large number of users in NOMA has resulted in a considerable improvement in the sum-rate, to the point that it has outperformed OFDMA with perfect CSI. Similar to NOMA, there is a limiting upper bound for OFDMA, which is reached at lower SNR values (e.g., 110 dB) as compared to NOMA (e.g., 130 dB).

Fig. 6 demonstrates how K impacts the sum-rate under different CSI error values. As expected for NOMA-VLC with perfect CSI, the number of users is directly proportional to the sum-rate, which increases from 6.4 bpcu to 7.8 bpcu when the number of users increased from 2 to 7. However, for the case of imperfect CSI, the performance gain becomes almost flat even at an increase in the number of users. This is a rather important observation since the imperfect CSI is highly disadvantageous for NOMA and a clear bottleneck. Yet, for OFDMA, even though it appears to be almost flat at a change from $K = 2$ to $K = 7$, it is noticed that the sum-rate decreases from 3 bpcu in the perfect CSI case to less than 0.72 bpcu and 0.59 bpcu for the cases of -120 dB and -130 dB, respectively. Likewise, Fig. 7 shows the impact of vertical distance from the LED on the NOMA-VLC sum-rate for different CSI error values. In the case of perfect CSI, there is an apparent reduction in the sum-rate from 3.76 bpcu at $L = 2$ to 2.8 bpcu at $L = 4.25$m. However, in the case of imperfect CSI with $\sigma_e = 10^{-12}$, the reduction ratio still
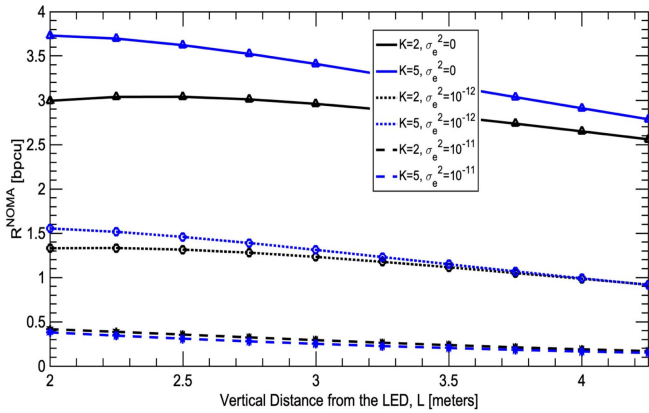
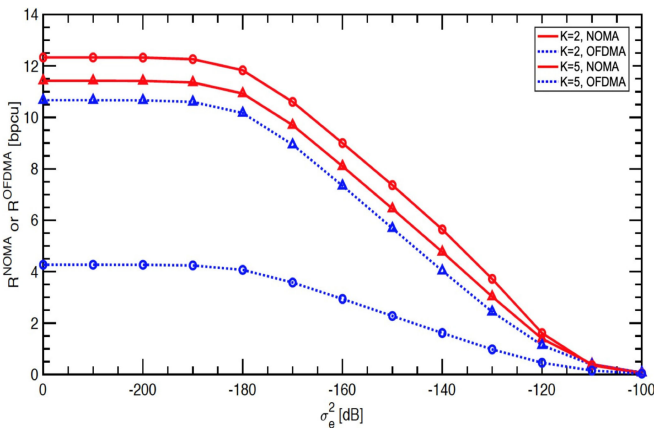Fig. 7.   Sum-rate vs. vertical distance from LED for NOMA-VLC.

Fig. 9.   Average energy efficiency vs. LOS availability probability with NOMA under different CSI conditions, with 4 users.

Fig. 8.   Sum-rate Vs CSI error (NOMA-VLC and OFDMA-VLC).

Fig. 10.   Average energy efficiency vs. power consumption of the VLC AP, under imperect CSI, with $K = 4$.

holds from 1.5 bpcu to 0.9 bpcu. This is expected because the channel correlation increases as the vertical length of the VLC AP increases and/or the number of users increases, i.e., $K \geq 5$. Finally, in the case of $\sigma_e = 10^{-12}$, the performance impact of L becomes smaller as it varies by 0.2 m.

Fig. 8 shows a comparison between the OFDMA-VLC and the NOMA-VLC sum-rate performance for the corresponding CSI error. It is evident that both cases are highly susceptible to incurred CSI errors, especially when $K = 5$. For NOMA-VLC with $K = 2$, the sum-rate drops from 11.4 bpcu to 0.06 bpcu, as the CSI error increases from -220 dB to -110 dB. Likewise, for OFDMA based VLC, there is a dramatic decrease, which is from 10.6 bpcu to 0.07 bpcu throughout the same CSI error range. Yet, the advantage of NOMA prevails when increasing the number of users from 2 to 5, in which case the achieved NOMA sum-rate increases from 11.4 bpcu to 12.3 bpcu. In contrast, OFDMA based sum-rate suffers from performance degradation as it decreasing from 10.6 bpcu to 4.6 bpcu due to the orthogonality.

B. Average Energy Efficiency of Hybrid NOMA Based RF/VLC

This subsection analyzes the average energy efficiency of the investigated hybrid VLC-RF system. In this setup, the room has a length and width of 4 meters and a height of 2.5 meters. The
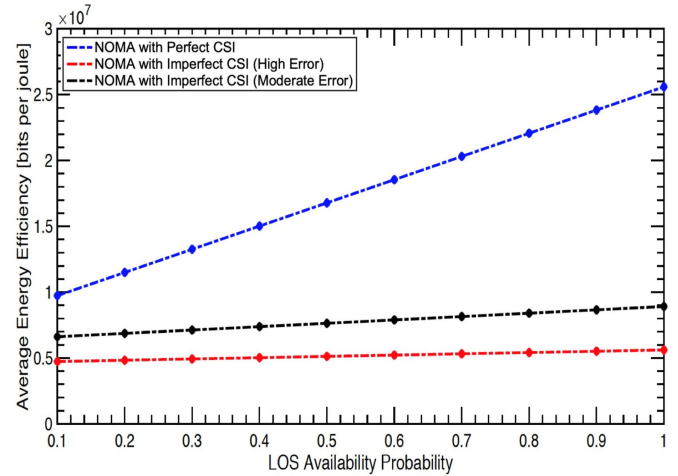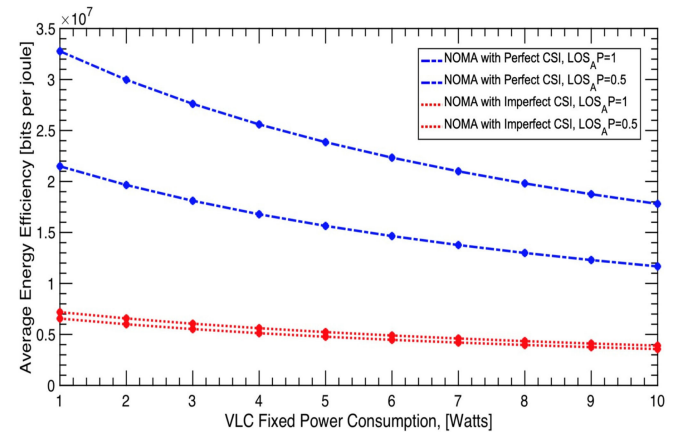
room has a single VLC AP in the ceiling, which has a fixed power consumption of 4 Watt and conversion efficiency of 1 Watt/Amps. Moreover, the room has a single RF AP with a fixed power consumption of 6.7 Watt [32]. The aim is to determine the average energy efficiency of the hybrid system under imperfect CSI, where the users are uniformly distributed and adopt a fixed power allocation policy. Finally, the transmit SNR is 150 dB for the VLC network and 30 dB for the RF network. At the same time, we assume an equal probability of LOS component availability for both types of AP, i.e., $\beta_{\text{VLC}} = \beta_{\text{RF}} = \beta$.

Fig. 9 illustrates the average energy efficiency as a function of the probability of LOS availability for the case of $K = 4$. It can be observed from Fig. 10 that higher LOS availability will lead to more performance drop caused by the imperfect CSI. For instance, when the LOS availability probability is 0.1, the average energy efficiency drops from 1×10^7 bit/J to 0.63×10^7 bit/J in the case of moderate CSI error, and to 0.48×10^7 bit/J in the case of high CSI error. However, in the case of full LOS availability, the average energy efficiency drops from 2.57×10^7 bit/J to 0.9×10^7 bit/J in the case of moderate CSI error, and to
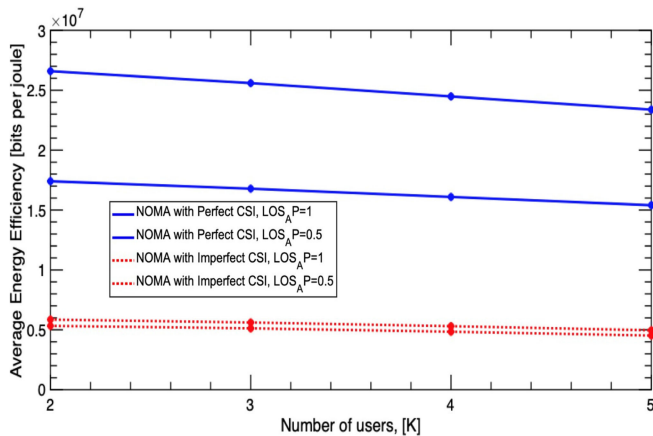
Fig. 11.   Average energy efficiency vs. number of users, under imperfect CSI.
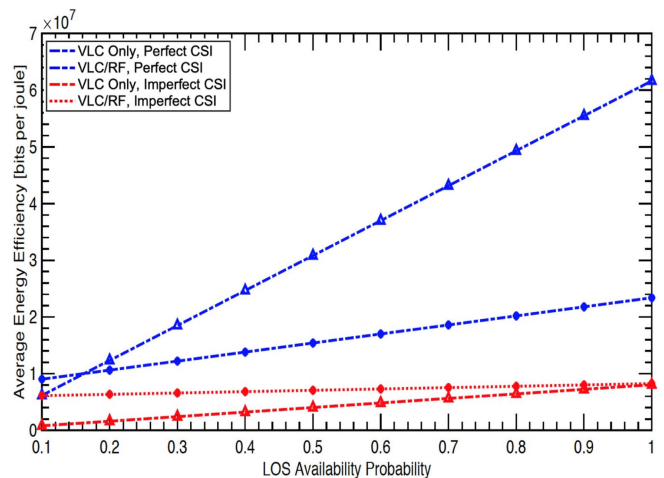

Fig. 12.   Average energy efficiency vs. LOS availability probability, using standalone VLC Scheme, and Hybrid VLC-RF Scheme, under imperfect CSI, with 4 users.

0.58×10^7 bit/J in the case of high CSI error. We can deduce that the imperfect CSI causes an incorrect ordering of the channel gains, which could lead to severe performance degradation in the system's performance. Therefore, and given that the effect of CSI errors is usually neglected, it is of paramount importance to take these effects into thorough consideration during practical designs of conventional VLC or hybrid VLC/RF systems.

Similarly, the average energy efficiency is illustrated in Fig. 10 versus VLC fixed power consumption, where we consider 2 LOS availability probability values, *i.e.* 0.5, and 1 at high CSI error. For the case of perfect CSI, the average energy efficiency increases considerably as we decrease the power consumption. However, for the imperfect CSI case, the average energy efficiency has highly deteriorated, and decreasing the power consumption is not effective; hence the curve is almost horizontal throughout the entire VLC power consumption range. For instance, the average energy efficiency reduced from 3.3×10^7 bit/J to 2.3×10^7 bit/J, which is almost a 30% drop. However, when the CSI is erroneous, the average energy efficiency is almost flat regardless of the power consumption. As a result, we can conclude that as the CSI error increases, reducing the VLC fixed power consumption will not result in any noticeable performance gain in terms of bits/J. Therefore, it is advised to mitigate the root cause of the issue, which is the CSI error.

Fig. 11 presents the average energy efficiency as a function of the number of users, using two LOS conditions (0.5 and 1), and with both perfect and imperfect high CSI error. It can be seen that the average energy efficiency is maintained around a certain value due to the non-orthogonality feature of NOMA, where all users utilize the entire bandwidth at the same time. This figure shows the clear advantage of NOMA over OFDMA. Moreover, two main observations can be drawn from this figure. First, the impact of LOS becomes negligible in case of high CSI error. For instance, in the case of 4 users with perfect CSI knowledge, the average energy efficiency decreases from 2.5×10^7 bit/J to 1.75×10^7 bit/J. However, in the case of imperfect CSI, the performance drops from 0.6×10^7 bit/J to 0.55×10^7 bit/J.

Finally, Fig. 12 demonstrates the average energy efficiency versus the LOS availability probability, under perfect CSI and highly erroneous CSI. In the case of perfect CSI, as expected,

the VLC-Only system outperforms the hybrid VLC-RF system when the probability of LOS availability is higher than 0.15. However, in the practical scenario where the CSI is imperfect, the advantages of the robust hybrid VLC-RF scheme are shown against the prone standalone VLC system. Notably, the average energy efficiency for the standalone VLC system with imperfect CSI is close to zero when there is a dominant NLOS scenario. However, for the hybrid VLC-RF system, the average energy efficiency withstands the severe LOS situation with an acceptable value of 0.77×10^7 bit/J. Moreover, as the LOS availability probability reaches 1 in the case of imperfect CSI, the average energy efficiency of both schemes meet at 0.9×10^7 bit/J. This means that the hybrid VLC-RF scheme is considerably more robust to withstand all the cases of LOS and can only be better when there is a partial LOS or can provide equal performance to the VLC-Only system when the LOS is fully available.

VII. Conclusion

This work evaluated the performance of a hybrid NOMA-VLC-RF system, assuming imperfect CSI and uniformly distributed users. Closed-form expressions were derived for the corresponding average sum-rate and average energy efficiency, which were extensively verified through comparisons with the respective computer simulation results. The results showed that the amount of CSI error has an impact on the performance of both NOMA and OFDMA schemes. The work demonstrated that the hybrid scheme of VLC-RF with NOMA is much more robust than the VLC-Only System with NOMA, under the case of imperfect CSI. Finally, the reported results can highly aid the design of practical hybrid VLC-RF systems.

References

[1] A. Al-Hammadi, S. Muhaidat, P. C. Sofotasios, and M. Al-Qutayri, "A robust and energy-efficient NOMA-enabled hybrid VLC/RF wireless network," in *Proc. IEEE Wireless Commun. Netw. Conf.*, Marrakech, Morocco, Apr. 2019, pp. 1–6.

[2] T. Asai, "5G radio access network and its requirements on mobile optical network," in *Proc. Int. Conf. Opt. Netw. Des. Model.*, Jun. 2015, pp. 7–11.

[3] J. G. *et al.*, "What will 5G be?," *IEEE J. Sel. Areas Commun.*, vol. 32, no. 6, pp. 1065–1082, Jun. 2014.

[4] C. Chang *et al.*, "A 100-Gb/s multiple-input multiple-output visible laser light communication system," *J. Lightw. Technol.*, vol. 32, pp. 4121–4127, 2014.

[5] C.-H. Chang *et al.*, "A 100-Gb/s multiple-input multiple-output visible laser light communication system," *J. Light. Technol.*, vol. 32, no. 24, pp. 4121–4127, Dec. 2014.

[6] Y. Lan, A. Benjebboiu, X. Chen, A. Li, and H. Jiang, "Considerations on downlink non-orthogonal multiple access (NOMA) combined with closed-loop SU-MIMO," in *Proc. Int. Conf. Signal Process.*, Jan. 2015, pp. 1–5.

[7] X. Chen, A. Benjebbour, Y. Lan, A. Li, and H. Jiang, "Impact of rank optimization on downlink non-orthogonal multiple access (NOMA) with SU-MIMO," in *Proc. IEEE Int. Conf. Commun. Syst.*, Nov. 2014, pp. 233–237.

[8] S. Timotheou and I. Krikidis, "Fairness for non-orthogonal multiple access in 5G systems," *IEEE Signal Process. Lett.*, vol. 22, no. 10, pp. 1647–1651, Oct. 2015.

[9] Z. Ding, F. Adachi, and H. V. Poor, "The application of MIMO to non-orthogonal multiple access," *IEEE Trans. Wireless Commun.*, vol. 15, no. 1, pp. 537–552, Jan. 2016.

[10] H. Marshoud, V. M. Kapinas, G. K. Karagiannidis, and S. Muhaidat, "Non-orthogonal multiple access for visible light communications," *IEEE Photon. Technol. Lett.*, vol. 28, no. 1, pp. 51–54, Jan. 2016.

[11] R. C. Kizilirmak, C. R. Rowell, and M. Uysal, "Non-orthogonal multiple access (NOMA) for indoor visible light communications," in *Proc. 4th Int. Workshop Opt. Wireless Commun.*, Sep. 2015, pp. 98–101.

[12] L. Yin, W. O. Popoola, X. Wu, and H. Haas, "Performance evaluation of non-orthogonal multiple access in visible light communication," *IEEE Trans. Commun.*, vol. 64, no. 12, pp. 5162–5175, Dec. 2016.

[13] G. Nauryzbayev, M. Abdallah, and H. Elgala, "On the performance of noma-enabled spectrally and energy efficient ofdm (SEE-OFDM) for indoor visible light communications," in *Proc. IEEE Veh. Technol. Conf. Spring*, Jun. 2018, pp. 1–5.

[14] H. Marshoud, P. C. Sofotasios, S. Muhaidat, G. K. Karagiannidis, and B. S. Sharif, "On the performance of visible light communication systems with non-orthogonal multiple access," *IEEE Trans. Wireless Commun.*, vol. 16, no. 10, pp. 6350–6364, Oct. 2017.

[15] H. Ma, L. Lampe, and S. Hranilovic, "Coordinated broadcasting for multiuser indoor visible light communication systems," *IEEE Trans. Commun.*, vol. 63, no. 9, pp. 3313–3324, Sep. 2015.

[16] K. Ying, H. Qian, R. Baxley, and S. Yao, "Joint optimization of precoder and equalizer in MIMO VLC systems," *IEEE J. Sel. Areas Commun*, vol. 33, no. 9, pp. 1949–1958, Sep. 2015.

[17] M. Rahaim, I. Abdalla, M. Ayyash, H. Elgala, A. Khreishah, and T. D. C. Little, "Welcome to the CROWD: Design decisions for coexisting radio and optical wireless deployments," *IEEE Netw.*, vol. 33, no. 5, pp. 174–182, Sep. 2019.

[18] S. Shao *et al.*, "Design and analysis of a visible-light-communication enhanced WiFi system," *IEEE J. Optical Commun. Netw.*, vol. 7, no. 10, pp. 960–973, Oct. 2015.

[19] Y. Wang and H. Haas, "Dynamic load balancing with handover in hybrid Li-Fi and Wi-Fi networks," *OSA J. Light. Technol.*, vol. 33, no. 22, pp. 4671–4682, Nov. 2015.

[20] X. Li, R. Zhang, and L. Hanzo, "Cooperative load balancing in hybrid visible light communications and WiFi," *IEEE Trans. Commun.*, vol. 63, no. 4, pp. 1319–1329, Apr. 2015.

[21] X. Bao, X. Zhu, T. Song, and Y. Ou, "Protocol design and capacity analysis in hybrid network of visible light communication and OFDMA systems," *IEEE Trans. Veh. Technol.*, vol. 63, no. 4, pp. 1770–1778, May 2014.

[22] J. Kong, M. Ismail, E. Serpedin, and K. A. Qaraqe, "Energy efficient optimization of base station intensities for hybrid RF/VLC networks," *IEEE Trans. Wireless Commun.*, vol. 18, no. 8, pp. 4171–4183, Aug. 2019.

[23] 3GPPTS36.300, "E-UTRA and E-UTRAN overall description, Stage 2," Accessed: Jan. 18, 2021. [Online]. Available: https://www.etsi.org/deliver/etsi_ts/136300_136399/136300/12.06.00_60/ts_136300v120600p.pdf

[24] H. Zhang, N. Liu, K. Long, J. Cheng, V. C. M. Leung, and L. Hanzo, "Energy efficient subchannel and power allocation for software-defined heterogeneous VLC and RF networks," *IEEE J. Sel. Areas Commun.*, vol. 36, no. 3, pp. 658–670, Mar. 2018.

[25] H. L. Yang, X. Z. Xie and M. Kadoch, "Intelligent resource management based on reinforcement learning for ultra-reliable and low-latency IoV communication networks," *IEEE Trans. Veh. Technol.*, vol. 68, no. 5, pp. 4157–4169, May 2019.

[26] H. L. Yang A. Alphones, C. Chen, W. D. Zhong, and X. Z. Xie, "Learning-based energy-efficient resource management by heterogeneous RF/VLC for ultra-reliable low-latency industrial IoT networks," *IEEE Trans. Ind. Inform.*, vol. 16, no. 8, pp. 5565–5576, Aug. 2020.

[27] A. Khreishah, S. Shao, A. Gharaibeh, M. Ayyash, H. Elgala, and N. Ansari, "A Hybrid RF-VLC system for energy efficient wireless access," *IEEE Trans. Green Commun. Netw.*, vol. 2, no. 4, pp. 932–944, Dec. 2018.

[28] V. K. Papanikolaou, P. D. Diamantoulakis, Z. Ding, S. Muhaidat, and G. K. Karagiannidis, "Hybrid VLC/RF networks with non-orthogonal multiple access," in *Proc. IEEE Global Commun. Conf.*, Dec. 2018, pp. 1–6.

[29] V. K. Papanikolaou, P. D. Diamantoulakis, P. C. Sofotasios, S. Muhaidat, and G. K. Karagiannidis, "On optimal resource allocation for hybrid VLC/RF networks with common backhaul," *IEEE Trans. Cogn. Commun. Netw.*, vol. 6, no. 1, pp. 352–365, Mar. 2020.

[30] X. Zhou, S. Li, Y. Wen, Y. Han, and D. Yuan, "Cooperative NOMA based VLC/rf system with simultaneous wireless information and power transfer," *IEEE Int. Conf. Commun. China*, Aug. 2018, pp. 100–105.

[31] Deep-Reinforcement-Learning-for-5G-Networks H. Chowdhury, I. Ashraf, and M. Katz, "Energy-efficient connectivity in hybrid radio-optical wireless systems," in *Proc. 10th Int. Symp. Wireless Wireless Commun. Syst.*, Aug. 2013, pp. 1–5.

[32] M. Kashef, M. Ismail, M. Abdallah, K. A. Qaraqe, and E. Serpedin, "Energy efficient resource allocation for mixed RF/VLC heterogeneous wireless networks," *IEEE J. Sel. Areas Commun.*, vol. 34, no. 4, pp. 883–893, Apr. 2016.

[33] Y. Saito, Y. Kishiyama, A. Benjebbour, T. Nakamura, A. Li, and K. Higuchi, "Non-orthogonal multiple access (NOMA) for cellular future radio access," in *Proc. IEEE 77th Veh. Technol. Conf.*, Jun. 2013, pp. 1–5.

[34] H. A. David and H. Nagaraja, *Order Statistics*, 3rd ed., Berlin, Germany: Springer, 2005, pp. 367–450, doi: 10.1002/0471722162.

[35] Z. Yang, Z. Ding, P. Fan, and G. K. Karagiannidis, "On the performance of non-orthogonal multiple access systems with partial channel information," *IEEE Trans. Commun.*, vol. 64, no. 2, pp. 654–667, Feb. 2016.

[36] A. P. Prudnikov, Yu. A. Brychkov, and O. I. Marichev, *Integrals and Series*, 3rd ed. New York, NY, USA: Gordon and Breach Science, vol. 1, Elementary Functions, 1992.

[37] H. L. Yang, X. Z. Xie and M. Kadoch, "Intelligent resource management based on reinforcement learning for ultra-reliable and low-latency IoV communication networks," *IEEE Trans. Veh. Technol.*, vol. 68, no. 5, pp. 4157–4169, May 2019.

[38] H. L. Yang A. Alphones, C. Chen, W. D. Zhong, and X. Z. Xie, "Learning-based energy-efficient resource management by heterogeneous RF/VLC for ultra-reliable low-latency industrial IoT networks," *IEEE Trans. Ind. Inform.*, vol. 16, no. 8, pp. 5565–5576, Aug. 2020.

[39] S. Ma, Y. He, H. Li, S. Lu, F. Zhang, and S. Li, "Optimal power allocation for mobile users in non-orthogonal multiple access visible light communication networks," *IEEE Trans. Commun.*, vol. 67, no. 3, pp. 2233–2244, Mar. 2019.

[40] X. Liu, Z. Chen, Y. Wang, F. Zhou, Y. Luo, and R. Q. Hu, "BER analysis of NOMA-enabled visible light communication systems with different modulations," *IEEE Trans. Veh. Technol.*, vol. 68, no. 11, pp. 10807–10821, Nov. 2019.

[41] Y. Yapici and I. Guvenc, "Non-orthogonal multiple access for mobile VLC networks with random receiver orientation," in *Proc. IEEE Global Commun. Conf.*, 2019, pp. 1–6.

[42] S. Ma, Y. He, H. Li, S. Lu, F. Zhang and S. Li, "Optimal power allocation for mobile users in non-orthogonal multiple access visible light communication networks," *IEEE Trans. Commun.*, vol. 67, no. 3, pp. 2233–2244, Mar. 2019.

Ahmed Al Hammadi (Member, IEEE) received the B.S. degree in electronics engineering in 2011 and the M.S. degree in communications engineering in 2015 from Khalifa University, Abu Dhabi, UAE, where he is currently working toward the Ph.D. degree in electrical and computer engineering. His current research interests include visible light communications and optimal power allocation techniques.

Paschalis C. Sofotasios (Senior Member, IEEE) was born in Volos, Greece, in 1978. He received the M.Eng. degree from Newcastle University, U.K., in 2004, the M.Sc. degree from the University of Surrey, U.K., in 2006, and the Ph.D. degree from the University of Leeds, U.K., in 2011. He has held academic positions with the University of Leeds, U.K., the University of California at Los Angeles, Los Angeles, CA, USA., Tampere University of Technology, Finland, Aristotle University of Thessaloniki, Greece, and Khalifa University, UAE, where he is currently an Assistant Professor with the Department of Electrical Engineering and Computer Science. His M.Sc. degree was funded by a scholarship from U.K.-EPSRC and his Ph.D. degree was sponsored by the U.K.-EPSRC and Pace plc.

His research interests include physical layer digital and optical wireless communications as well as in topics relating to special functions and statistics. He received the Best Paper Award at ICUFN 2013. He received the Exemplary Reviewer Award from IEEE COMMUNICATIONS LETTERS in 2012 and theIEEE TRANSACTIONS ON COMMUNICATIONS in 2015 and 2016. He is an Editor of IEEE COMMUNICATIONS LETTERS. He is a Regular Reviewer for several international journals and has been a Member of the Technical Program Committee of numerous IEEE conferences.

Mahmoud Al-Qutayri (Senior Member, IEEE) received the B.Eng. degree in electrical and electronic engineering from Concordia University, Canada, in 1984, the M.Sc. degree in electrical and electronic engineering from the University of Manchester, U.K., in 1987, and the Ph.D. degree in electrical and electronic engineering from the University of Bath, U.K., in 1992. He is currently a Full Professor with the Department of Electrical and Computer Engineering and the Associate Dean of Graduate Studies, College of Engineering, Khalifa University, UAE. Prior to joining Khalifa University, he was with De Montfort University, U.K. and University of Bath, U.K. He has authored or coauthored numerous technical papers in peer-reviewed journals and international conferences. He also coauthored a book entitled *Digital Phase Lock Loops: Architectures and Applications* and edited a book entitled *Smart Home Systems*, and a number of book chapters and patents. His current research interests include wireless sensor networks, embedded systems design, in-memory computing, mixed-signal integrated circuits design and test, and hardware security.

Sami Muhaidat (Senior Member, IEEE) received the Ph.D. degree in electrical and computer engineering from the University of Waterloo, Waterloo, ON, Canada, in 2006. From 2007 to 2008, he was an NSERC Postdoctoral Fellow with the Department of Electrical and Computer Engineering, University of Toronto, Canada. From 2008 to 2012, he was an Assistant Professor with the School of Engineering Science, Simon Fraser University, BC, Canada. He is currently a Professor with Khalifa University and an Adjunct Professor with Carleton University, Ontario, Canada. His research interests include advanced digital signal processing techniques for wireless communications, RIS, 5G and beyond, MIMO, optical communications, IoT with emphasis on battery-free devices, and machine learning. He is currently an Area Editor of the IEEE TRANSACTIONS ON COMMUNICATIONS and Lead Guest Editor of the IEEE OPEN JOURNAL OF THE COMMUNICATIONS SOCIETY "Large-Scale Wireless Powered Networks with Backscatter Communications" Special Issue. He was a Senior Editor and Editor of the IEEE COMMUNICATIONS LETTERS, an Editor of the IEEE TRANSACTIONS ON COMMUNICATIONS, and an Associate Editor for the IEEE TRANSACTIONS ON VEHICULAR TECHNOLOGY.

Hany Elgala (Senior Member, IEEE) received the Ph.D. degree from Jacobs University, Germany, in 2010. He was a Research Professor with Boston University, MA, USA. He is an Assistant Professor with the Electrical and Computer Engineering Department, University at Albany - State University of New York, USA. He was a Faculty Member and a Communications Testbed Leader with the Light Enabled Systems & Applications, Engineering Research Center. He has authored or coauthored more than 80 journal and conference publications, several patents, and a book chapter entitled *Dimming and Modulation for VLC-Enabled Lighting*. He works in the area of wireless networks, digital signal processing, and embedded systems. He has been active in visible light communications research for more than 12 years, including OFDM modulation, MIMO transmission, coexistence with RF technologies and nonlinearity. He is currently an Editor of the IEEE TRANSACTIONS ON COMMUNICATIONS for Optical Wireless Systems and Networks. He was a Guest Editor of the IEEE ACCESS Special Section: Optical Wireless Technologies for 5G Communications and Beyond the TPC Member for conferences and symposia, including the IEEE Optical Networks and Systems Symposium and Workshop on Optical Wireless Communications at GLOBECOM from 2012 to 2015.